Hindawi
International Journal of Chemical Engineering
Volume 2021, Article ID 5179268, 8 pages
https://doi.org/10.1155/2021/5179268

*Research Article*

# A Novel Mass Transfer Model to Describe the Separation Process in Reverse Osmosis of Glucose

**Chenghan Chen**,[1] **Yanwei Wang**,[1] **Furong Tan**,[1] **and Qili Zhu**[2]

[1]*Team of Straw Utilization, Biogas Institute of Ministry of Agriculture and Rural Affairs, Chengdu 610041, China*
[2]*Department of Biological Functions Engineering, Graduate School of Life Science and Systems Engineering, Kyushu Institute of Technology, 2-4 Hibikino, Wakamatsu, Kitakyushu 808-0196, Japan*

Correspondence should be addressed to Chenghan Chen; chenchenghan@caas.cn

Received 19 October 2021; Revised 10 December 2021; Accepted 15 December 2021; Published 26 December 2021

Academic Editor: João Claudio Thomeo



Basic and theoretical research on processes such as reverse osmosis (RO) is essential in the fermentation industry to improve production efficiency and reduce cost. Here, we focus on the RO concentration of glucose solutions. We constructed a mathematic model that incorporates various membrane and experimental parameters to characterize the mass transfer process of RO membrane and validated the model output with experimental data. Calculation results were highly consistent with the experimental data, demonstrating that this model can be useful for predicting the RO concentration process.

## 1. Introduction

The field of fermentation technology has rapidly advanced over recent years [1]. In the microbial fermentation process, the concentration of fermentable sugar is a key component that directly impacts the ultimate concentration of target products [2]. Low concentrations of fermentable sugar in the fermentation broth lead to low concentrations of the target product, and the subsequent purification process is expensive [3]. As such, it is important to increase the concentrations of fermentable sugars prior to fermentation.

Many methods to concentrate fermentable sugars have been developed, including vacuum distillation [4], pervaporation [5], and freezing [6]. In general, these techniques are useful [7], but typically usually involve complicated operations performed by expensive equipment with high energy demands. This industry urgently needs to develop a convenient and environment-friendly in situ concentration method. Here, we present membrane technology as a feasible alternative.

Widespread interest has developed in the use of membrane technology as a sugar concentration method. In recent years, this technique has become widely adopted in industrial applications and research laboratories as it is energy saving, environment friendly, and exhibits permselectivity capability [8–10]. At present, biorefining uses pressure-, chemical-, or thermal-driven membrane systems such as RO, microfiltration (MF), ultrafiltration (UF), nanofiltration (NF), pervaporation (PV), and membrane distillation (MD) to concentrate sugars [11]. Of these, NF and RO have been successfully employed to concentrate glucose and xylose [12]; however, RO membranes are more efficient as they possess pore sizes that more effectively prevent sugar loss [13].

Increased focus on RO technology has resulted in a high demand for RO membranes, elevating the cost of RO systems. Optimizing the RO membrane can reduce these costs. One method of making the system more efficient is to develop a mathematical model that adequately describes the performance of the RO process [14]. On the other hand, the concentration of sugar in the concentrate is an important parameter in the RO concentration process. Therefore, further research needs to be carried out to reveal the impact of various parameters in the RO process on the sugar concentration process, including membrane parameters and experimental parameters.

Here, we investigated the mass transfer glucose during the RO process by carrying out a series of concentration experiments using glucose in a laboratory-scale RO system. With the results from these experiments, we developed a novel mathematical model that comprehensively reflects the effect of various parameters to characterize the mass transfer process of the RO membrane. Studies on validation of the model with experimental results were carried out. This model will provide valuable information that can be used to predict the RO concentration process.

## 2. Experimental

*2.1. Membrane and Module.* RO membranes are comprised primarily of polyamide and cellulose acetate (CA). Nowadays, polyamide membranes dominate RO market sales with a 91% share, with asymmetric CA hollow fiber membranes holding a distant second spot. Although the latter has superior chlorine resistance, the former has higher salt rejection and net pressure driving force [15]. A polyamide composite membrane (PA2-4040, HYDECANME, USA) was selected for the experiments (see Table 1 for characteristics of the membrane).

The experimental setup (Figure 1) consisted of a cooling and heating circulation tank to control the temperature of the model solution, a pump for feeding glucose solution into the membrane module, a check valve to control the solution flux, the RO membrane module which included pressure gauges and a flow meter, and a device for sampling the solution.

*2.2. Model Solution Preparation.* In this study, glucose anhydrous (AR) was purchased from Kelong Chemical Reagent Factory, Chengdu, China. Model solutions (24.8–166.8 mol•$m^{-3}$) were prepared using ultrapure water, adding suitable amounts of the analytes (calculated).

*2.3. Concentration Experiment.* The glucose model solutions were selected to carry out RO concentration experiments (Figure 1). In this experiment, the RO membrane remained unchanged. Prior to running the experiment, the system was flushed with deionized water. Model solutions (15 L) were transferred into the membrane module using a feed pump. Next, the solution was concentrated and permeate outflow from the RO membrane module was recirculated into the circulation tank. A series of operation parameters were examined during this procedure, including glucose solution inlet flux ($Q_f$, $28 \times 10^{-6}\ m^3\ s^{-1} < Q_f < 250 \times 10^{-6}\ m^3\ s^{-1}$, obtained using a flowmeter), inlet concentration of glucose solution ($C_f$, $35\ mol\ m^{-3} < C_f < 140\ mol\ m^{-3}$, calculated), transmembrane pressure ($\triangle p$, $300\ kPa < \triangle p < 620\ kPa$, obtained using a pressure gauge), and temperature ($T$, $T = 306$ K, obtained using a temperature gauge). Samples were collected three times to obtain an average value under each experimental condition.

In this study, membrane performance was evaluated by the observed retention. The observed retention is displayed as $R_o$ and characterizes the ability of the $R_o$ membrane to retain a component, where the greater the $R_o$ value, the greater the difficulty to pass through the membrane. $R_o$ can be expressed by the following equation [16]:

$$R_o = \frac{C_f - C_p}{C_f}, \quad (1)$$

where $C_f$ (g·$L^{-1}$) and $C_p$ (g·$L^{-1}$) are the feed concentration and permeate concentration of the solute.

*2.4. Assay.* The concentration of glucose solutions (amount of sample for each test: 20 μL) was quantified by high-performance liquid chromatography (HPLC, Agilent LC1200, USA) equipped with a differential refraction detector (RID), and an Aminex HPX-87H column (Bio-Rad Co., Hercules, CA, USA). The mobile phase was 5 mmol $L^{-1}$ $H_2SO_4$ at a flow rate of 0.6 mL·$min^{-1}$, and the column temperature was maintained at 35°C.

## 3. Results and Discussion

*3.1. RO Experiments.* To obtain the membrane performance in the process of RO concentration experiments, some operation parameters were examined. Transmembrane pressure and feed flow were found to interact with each other, with flow rate decreasing as transmembrane pressure increased (Figure 2). The feed flow was changed by adjusting valve 1, and transmembrane pressure in the system was changed by adjusting valve 2 and valve 3.

When other experimental conditions were held constant (feed solution concentration $C_f = 70.17\ mol\ m^{-3}$, PH = 6, and feed solution temperature $T = 306$ K), the total flux of solvent and solute $J_v$, $R_o$, and concentrate solution concentration $C_b$ decreased with feed solution flow (Figure 3). $R_o$ slightly decreased with the increase of $Q_f$ (Figure 3(a)). $\triangle p$ also decreased with $Q_f$, which mean that a unit volume of feed solution can be divided into less pressure to facilitate the RO process, and the macroscopic performance of this process was the decrease in $R_o$ and $J_v$ (Figure 2). As $Q_f$ increased, the rate of $C_b$ reduction changed from fast to slow (Figure 3(b)). Overall, $J_v$ decreased with $Q_f$, which means the concentrate flow $Q_b$ increased as $Q_f$ increased, and the $Q_b$ was close to $Q_f$; then, $C_b$ also approached $C_f$ (Figure 3(a)). If $Q_f$ continues to increase, two consequences may result: (1) $Q_f$ exceeds the processing capacity of the membrane, resulting in membrane damage; (2) $C_b$ becomes approximately the same as $C_f$ such that the RO process substantially loses the ability to separate.

An increase in $C_f$ led to increases in $C_b$ and decreases in $J_v$ (Figure 4). RO did not detectably vary with $C_f$. In the RO process, concentration polarization (CP) is a phenomenon where the solute accumulates on the surface of the membrane causing substantial reduction in the rejection coefficient of the membrane. When $Q_f$ is constant, the increase in $C_f$ led to severe CP, decreasing $J_v$. In addition, high levels of CP led to a slightly lower trend of $R_o$. $C_b$ also increased with $C_f$, as predicted.

Overall, we found that different operating parameters have different effects on $C_b$ and are difficult to quantify

Table 1: Main characteristics of the used membrane.

| Type | PA2-4040 | |
|---|---|---|
| Membrane properties | Composition | Polyamide |
| | Permeable capacity (average, $m^3 \cdot d^{-1}$); membrane area effectively ($m^2$) | 7.2; 7.9 |
| | Recovery rate (single, %) | 15 |
| Usage conditions | Maximum pressure (Mpa) | 4.14 |
| | Temperature (°C) | 5–45 |
| | Maximum flow ($m^3 \cdot h^{-1}$) | 3.6 |

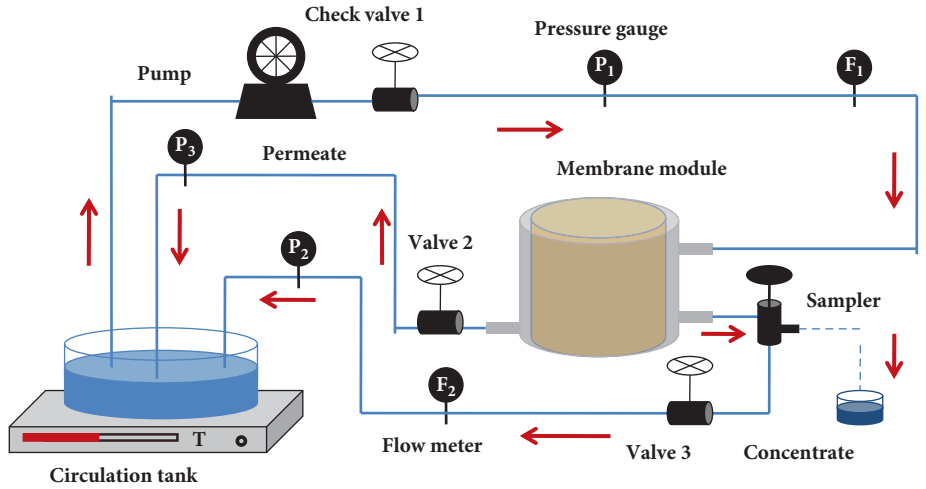


Figure 1: Schematic illustration of the RO system.

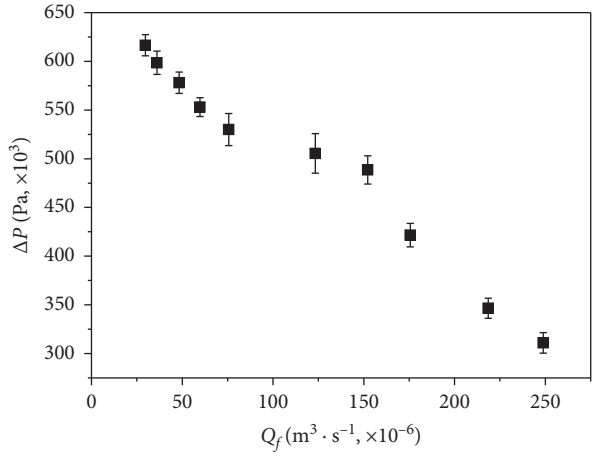


Figure 2: Relation between transmembrane pressure and feed solution flow ($C_f = 70.17\ \text{mol m}^{-3}$, PH = 6, and $T = 306\ \text{K}$).

(Figures 3 and 4). Therefore, this paper aims to derive a mathematical model that can synthesize various parameters to better express $C_b$.

*3.2. Membrane Transport Equations.* Mass transfer in RO separation processes is mainly governed by two aspects, (1) inside-membrane mass transfer and (2) outside-membrane mass transfer. In outside-membrane mass transfer, the main object of investigation is the mass transfer process near the membrane, which can be significantly hindered by CP (Figure 5). The relationship of solute concentration at the membrane surface, feed solution concentration, and permeate solution concentration can be expressed by the following equation [17]:

$$\frac{C_{\delta,1} - C_p}{C_f - C_p} = e^{\left(J_w \delta_{c,p}/D\right)} = e^{\left(J_w/k\right)}, \tag{2}$$

where $J_w$ is the solvent (pure water) flux, $C_p$ is the permeate solution concentration, $D$ is the diffusion coefficient, $C_{\delta,1}$ is the solute concentration at the membrane surface (feed side,

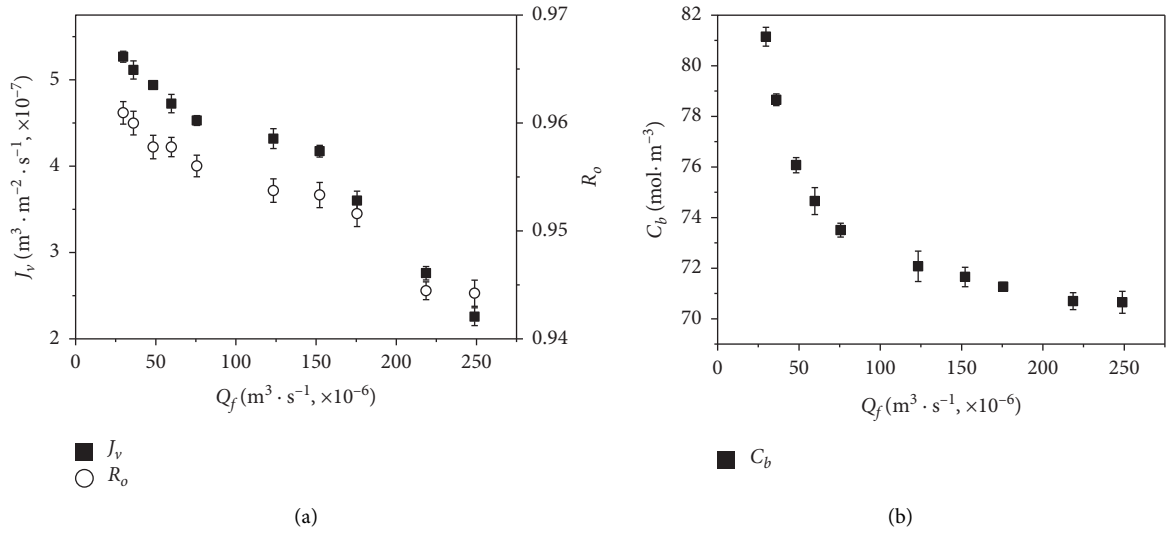


Figure 3: Influence of feed solution flow on the solvent flux, solute rejection, and concentrate solution concentration. ($C_f = 70.17$ mol $m^{-3}$, PH = 6, and $T = 306$ K).

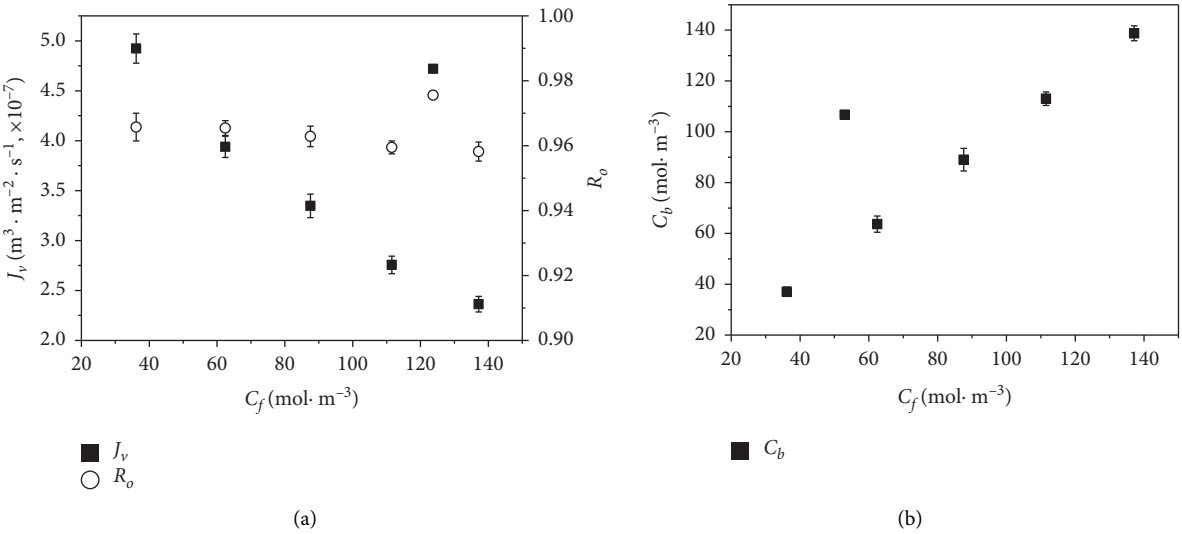


Figure 4: Influence of feed solution concentration on the solvent flux, solute rejection, and concentrate solution concentration ($Q_f = 1.56 \times 10^{-4}$ $m^3$ $s^{-1}$, PH = 6, and $T = 306$ K).

Figure 5), $\delta_{cp}$ is the $C_P$ layer thickness, and $k$ is the mass transfer coefficient in the CP layer.

For the RO process, the relationship between the solute flux $J_s$, $J_w$ , and $J_v$ is as follows:

$$J_v = J_w + J_s \approx J_w. \tag{3}$$

To describe the mass transfer process of inside-membrane, the irreversible thermodynamic Spiegler–Kedem model [18, 19] is assumed to be appropriate to explain the separation performance of solute through the membrane in this work. As much, $J_v$ can be expressed by the following equation:

$$J_v = L_p + (\Delta p - \sigma \Delta \pi), \tag{4}$$

where $L_p$ is the hydraulic permeability constant, $\triangle\pi$ is the difference in the osmotic pressure across the membrane, and $\sigma$ is the reflection coefficient. The reflection coefficient represents the solute separation capability of a membrane, which, for permeable membranes, is bounded by 0<puncsp> </puncsp><<puncsp> </puncsp>$\sigma < 1$. $\triangle\pi$ is calculated using the following equation:

$$\Delta \pi = RT\left(C_{\delta,1} - C_{\delta,2}\right) = RT\left(C_{\delta,1} - C_p\right), \tag{5}$$

where $R$ is the gas law constant, $T$ is the temperature, and $C_{\delta,2}$ is the solute concentration at the membrane surface (permeate side, Figure 5).

Substituting equation (5) in equation (4), we get

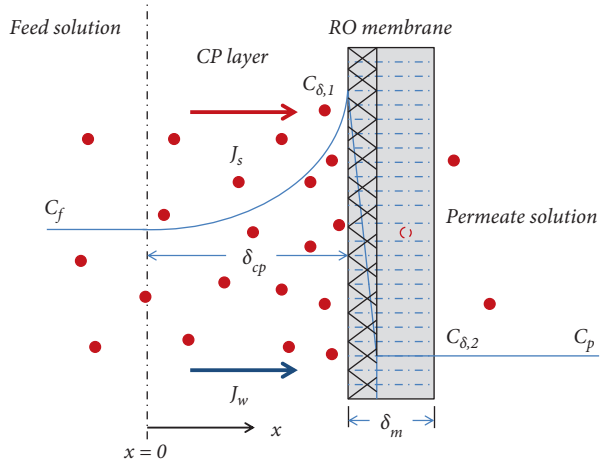


FIGURE 5: Schematic diagram of the mass transfer in $R_o$ membrane separation process.

$$J_v = L_p(\Delta p - \sigma\Delta\pi) = L_p\left[\Delta p - \sigma RT\left(C_{\delta,1} - C_p\right)\right]. \quad (6)$$

*3.3. Conservation Equations.* According to the principle of mass conservation, we can get the following equations:

$$Q_f C_f = Q_b C_b + Q_p C_p, \quad (7)$$

$$Q_f = Q_b + Q_p, \quad (8)$$

where $Q_p$ is the permeate flow. Also, the relationship between $Q_p$ and $J_v$ is shown in the following equation:

$$J_v = \frac{Q_p}{s}, \quad (9)$$

where $S$ is the $R_o$ membrane area effectively.

Substituting equations (8) and (9) in equation (7), we can get an equation for $C_b(L)$ at the exit:

$$C_b(L) = \frac{Q_f C_f}{Q_f - J_v S} - \frac{J_v S}{Q_f - J_v S} C_P. \quad (10)$$

Substituting equation (6) in equation (10), we get

$$C_b(L) = \frac{Q_f C_f - C_p L_p\left[\Delta p - \sigma RT\left(C_{\delta,1} - C_p\right)\right]S}{Q_f - C_p\left[\Delta p - \sigma RT\left(C_{\delta,1} - C_p\right)\right]S}. \quad (11)$$

Since $C_{\delta,1}$ is difficult to determine, the key to solving $C_b$ is to express $C_{\delta,1}$–$C_p$.

*3.4. Flow Equations.* According to equations (7) and (8), we can get the following equations:

$$Q_f C_f = Q_b(x)C_b(x) + Q_p(x)C_p(x), \quad (12)$$

$$Q_f = Q_b(x) + Q_p(x). \quad (13)$$

As the concentration of the permeate solution concentration in the RO process is small, $C_p$ is assumed to be uniform in the permeate channel and can, therefore, be expressed as a constant. Thus, equation (12) can be rewritten as

$$Q_f C_f = Q_b(x)C_b(x) + Q_p(x)C_p. \quad (14)$$

According to Figure 6, the total mass balance and the solute mass balance at any point along the feed channel are given as follows [20]:

$$\frac{du_b(x)}{dx} = -\frac{J_v}{h_f}, \quad (15)$$

$$\frac{dC_b(x)}{dx} = -\frac{J_v}{u_b h_f}\left[C_b(x) - C_{\delta,1}(x)\right], \quad (16)$$

where $u_b$ and $h_f$ are the feed solution flow rate and feed channel thickness.

According to equations (13) and (15), we get

$$\frac{dQ_b(x)}{dx} = -\frac{dQ_p(x)}{dx}, \quad (17)$$

$$\frac{dQ_b(x)}{dx} = \frac{du_b(x)}{dx}A = -\frac{J_v}{h_f}wh_f = -wJ_v, \quad (18)$$

where $A$ and $w$ are the feed channel cross-sectional area and feed channel width.

Also, according to equation (16), we get

$$0 = \frac{dQ_b(x)}{dx}C_b(x) + \frac{dC_b(x)}{dx}Q_b(x) + \frac{dQ_p(x)}{dx}C_p. \quad (19)$$

Substituting equations (16), (17), and (18) in equation (19), we get

$$2C_b(x) = C_{\delta,1}(x) + C_p. \quad (20)$$

We define $\varphi = C_{\delta,1}(L) - C_p$; then, equation (20) can be rewritten as follows:

$$C_b(L) = \frac{\varphi + 2C_p}{2}. \quad (21)$$

Combining equations (11) and (21), we can get the following expression:

$$\left[\varphi + \frac{1}{2}\left(\frac{Q_f - L_p\Delta pS}{L_pS\sigma RT}\right)\right]^2 = \frac{2Q_f\left(C_f - C_p\right)}{L_pS\sigma RT} + \frac{1}{4}\left(\frac{Q_f - L_p\Delta pS}{L_pS\sigma RT}\right)^2. \quad (22)$$

Then, we can derive the expression of $\varphi$:

$$\varphi = \frac{\sqrt{\theta} - \left(Q_f - L_p\Delta pS\right)}{2L_pS\sigma RT}. \quad (23)$$

We define $\theta$ as follows:

$$\theta = 8Q_f\left(C_f - C_p\right)L_pS\sigma RT + \left(Q_f - L_p\Delta pS\right)^2. \quad (24)$$

According to equations (21) and (23), we can get the concentrate solution concentration at the exit as the following expression:

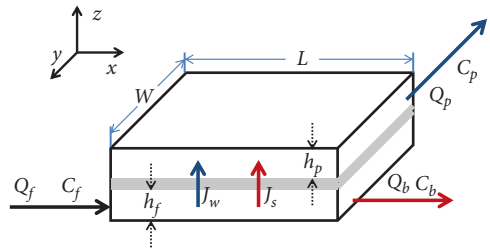


Figure 6: Schematic diagram of macroseparation process in the $R_o$ membrane.

Table 2: Calculated value of $L_p$ ($C_f = 70.17\,\text{mol m}^{-3}$, PH = 6, $T = 306\,\text{K}$, and $R = 8.314\,\text{J mol}^{-1}\,\text{K}^{-1}$).

| $Q_f$ ($\text{m}^3\ \text{s}^{-1}$, $\times 10^{-6}$) | $\triangle p$ (Pa, $\times 10^3$) | $C_p$ ($\text{mol m}^{-3}$) | $Lp$ ($\text{m·s}^{-1}\,\text{Pa}^{-1} \times 10^{-12}$) |
|---|---|---|---|
| 248.8889 | 311 | 3.9142 | 1.3923 |
| 218.6111 | 346.5 | 3.8976 | 1.3611 |
| 175.5556 | 421.5 | 3.3972 | 1.3423 |
| 152.2222 | 488.5 | 3.2748 | 1.3238 |
| 123.3333 | 505.5 | 3.2471 | 1.3048 |
| 75.5556 | 530 | 3.0858 | 1.3889 |
| 59.7222 | 553 | 2.9635 | 1.3709 |
| 48.3333 | 578 | 2.9635 | 1.3538 |
| 36.1111 | 598.5 | 2.8078 | 1.353 |
| 29.7222 | 616.5 | 2.7411 | 1.3529 |

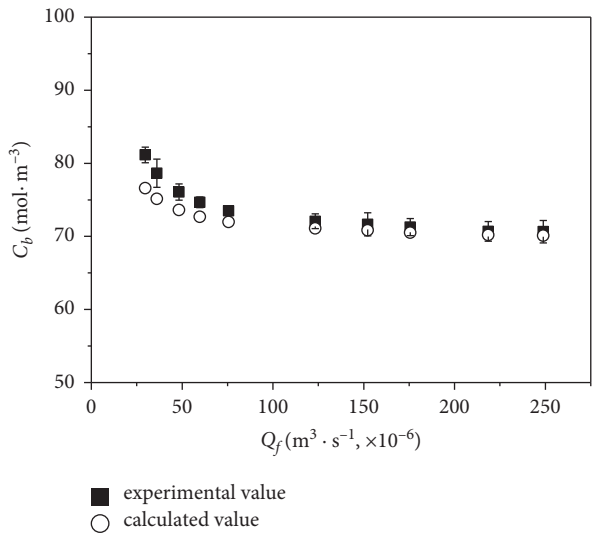


Figure 7: Comparison of the two $C_b$.

$$C_b(L) = \frac{2Q_fC_f - Q_fC_p - L_p\Delta pSC_p + C_p\sqrt{\theta}}{Q_f - L_p\Delta pS + \sqrt{\theta}}. \quad (25)$$

According to equation (25), the concentrate solution concentration $C_b$ at the exit is related to $C_f$ and $C_p$, membrane parameters $L_p$, $\sigma$, and $S$, and operating parameters $Q_f$, $T$, and $\triangle p$. When these parameters are known, $C_b$ can be calculated.

*3.5. Model Validation.* In this section, model validation needs to be carried out to verify whether the calculated values of the mathematical formula $C_b$ is consistent with experimental data. First, we need to determine the parameter values used in the model from our experimental system. The nonlinear parameter estimation technique with Levenberg–Marquardt with Gauss–Newton algorithm [21, 22] was used to determine these parameters. The calculated value of $\sigma$ is 0.9981. $L_p$, values were also calculated and found to remain constant across within the range of experimental parameters (Table 2).

The concentrate solution concentration $C_b$ from our experiment was obtained using HPLC. The theoretical value of $C_b$ was also calculated based on equation (20). The

comparison of the two $C_b$ value is shown in Figure 7. The relative error between treatment and theoretical $C_b$ values was calculated, and the maximum value of the relative error was found to be 5.62%.

## 4. Conclusions

Reverse osmosis (RO) concentration of glucose solution was studied to provide information that can improve the fermentation efficiency and reduce cost. To describe the concentration process, a mathematical model that accurately incorporates the effects of various parameters was developed to characterize the mass transfer process of the RO membrane. Comparison between experimental findings and model results revealed that the calculated concentrate solution concentration was consistent with the experimental data within 5.62%. This model can be used to predict the RO concentration process.

## Data Availability

The data used to support the findings of this study are included within the article.

## Conflicts of Interest

The author declares that there are no conflicts of interest regarding the publication of this paper.

## Acknowledgments

This work was supported by the Sichuan Science and Technology Program (grant nos. 2020YFN0015 and 2020YFH0021]; the Central Public-Interst Scientific Institution Basal Research fund (grant no. Y2019LM02); and the Local financial funds of National Agricultural Science and Technology Center (grant no. NASC2019TI06).

## References

[1] I. B. Nogueira, R. Dayana Montero, A. Rosildeide da Silva, L. Amanda Barbosa, and B. Ana Paula, "Bioconversion of agroindustrial waste in the production of bioemulsifier by Stenotrophomonas maltophilia UCP 1601 and application in bioremediation process," *International Journal of Chemical Engineering*, vol. 2020, 2020.

[2] M. A. Alam, T. Yuan, W. Xiong, B. Zhang, Y. Lv, and J. Xu, "Process optimization for the production of high-concentration ethanol with Scenedesmus raciborskii biomass," *Bioresource Technology*, vol. 294, Article ID 122219, 2019.

[3] K. Öhgren, R. Andreas, G. Mats, and Z. Guido, "Fuel ethanol production from steam-pretreated corn stover using SSF at higher dry matter content," *Biomass and Bioenergy*, vol. 30, no. 10, pp. 863–869, 2006.

[4] K. Srilekha Yadav, S. Naseeruddin, G. Sai Prashanthi, L. Sateesh, and L. Venkateswar Rao, "Bioethanol fermentation of concentrated rice straw hydrolysate using co-culture of *Saccharomyces cerevisiae* and Pichia stipitis," *Bioresource Technology*, vol. 102, no. 11, pp. 6473–6478, 2011.

[5] Q. Kang, B. Van der Bruggen, R. Dewil, J. Baeyens, and T. Tan, "Hybrid operation of the bio-ethanol fermentation," *Separation and Purification Technology*, vol. 149, pp. 322–330, 2015.

[6] V. Rooni, M. Raud, and T. Kikas, "The freezing pre-treatment of lignocellulosic material: a cheap alternative for Nordic countries," *Energy*, vol. 139, pp. 1–7, 2017.

[7] Y. Liu, Y. Zhang, J. Xu, Y. Sun, Z. Yuan, and J. Xie, "Consolidated bioprocess for bioethanol production with alkali-pretreated sugarcane bagasse," *Applied Energy*, vol. 157, pp. 517–522, 2015.

[8] A. Fayet, A. R. S. Teixeira, F. Allais, M. Bouix, and M.-L. Lameloise, "Detoxification of highly acidic hemicellulosic hydrolysate from wheat straw by dianafiltration with a focus on phenolic compounds," *Journal of Membrane Science*, vol. 566, pp. 112–121, 2018.

[9] K. Ueno, H. Negishi, T. Okuno et al., "High-performance silicalite-1 membranes on porous tubular silica supports for separation of ethanol/water mixtures," *Separation and Purification Technology*, vol. 187, pp. 343–354, 2017.

[10] M. Shibuya, K. Sasaki, Y. Tanaka et al., "Development of combined nanofiltration and forward osmosis process for production of ethanol from pretreated rice straw," *Bioresource Technology*, vol. 235, pp. 405–410, 2017.

[11] P. Pal, R. Kumar, A. K. Ghosh, and G. Alak Kumar, "Analysis of process intensification and performance assessment for fermentative continuous production of bioethanol in a multi-staged membrane-integrated bioreactor system," *Energy Conversion and Management*, vol. 171, pp. 371–383, 2018.

[12] L. Pan, M. He, B. Wu, Y. Wang, G. Hu, and K. Ma, "Simultaneous concentration and detoxification of lignocellulosic hydrolysates by novel membrane filtration system for bioethanol production," *Journal of Cleaner Production*, vol. 227, pp. 1185–1194, 2019.

[13] F. Zhou, C. Wang, and J. Wei, "Separation of acetic acid from monosaccharides by NF and RO membranes: performance comparison," *Journal of Membrane Science*, vol. 429, pp. 243–251, 2013.

[14] S. Sundaramoorthy, G. Srinivasan, and D. V. R. Murthy, "An analytical model for spiral wound reverse osmosis membrane modules: Part I - model development and parameter estimation," *Desalination*, vol. 280, no. 1-3, pp. 403–411, 2011.

[15] K. P. Lee, T. C. Arnot, and D. Mattia, "A review of reverse osmosis membrane materials for desalination-Development to date and future potential," *Journal of Membrane Science*, vol. 370, no. 1-2, pp. 1–22, 2011.

[16] C. Chen, K. Ma, Q. Zhu et al., "A method for concentration of monosaccharide and removal of inhibitors during hydrolysate pretreatment for improved bioethanol production," *Journal of Cleaner Production*, vol. 260, Article ID 120999, 2020.

[17] C. Chen and H. Qin, "A mathematical modeling of the reverse osmosis concentration process of a glucose solution," *Processes*, vol. 7, no. 5, Article ID 271, 2019.

[18] A. Śl□zak, "Irreversible thermodynamic model equations of the transport across a horizontally mounted membrane," *Biophysical Chemistry*, vol. 34, no. 2, pp. 91–102, 1989.

[19] D. Van Gauwbergen and J. Baeyens, "Modelling reverse osmosis by irreversible thermodynamics," *Separation and Purification Technology*, vol. 13, no. 2, pp. 117–128, 1998.

[20] E. Dimitriou, P. Boutikos, E. S. Mohamed, S. Koziel, and G. Papadakis, "Theoretical performance prediction of a reverse osmosis desalination membrane element under variable operating conditions," *Desalination*, vol. 419, pp. 70–78, 2017.

[21] D. W. Marquardt, "An algorithm for least-squares estimation of nonlinear parameters," *Journal of the Society for Industrial and Applied Mathematics*, vol. 11, no. 2, pp. 431–441, 1963.

[22] J. Dong, K. Lu, J. Xue, S. Dai, R. Zhai, and W. Pan, "Accelerated nonrigid image registration using improved Levenberg-Marquardt method," *Information Sciences*, vol. 423, pp. 66–79, 2018.